Deposition of TiO$_2$ Thin Films on Wood Substrate by an Air Atmospheric Pressure Plasma Jet

Ghiath Jnido *, Gisela Ohms and Wolfgang Viöl (ORCID)

Laboratory of Laser and Plasma Technologies, University of Applied Sciences and Arts, Von-Ossietzky-Straße 99, 37085 Göttingen, Germany

* Correspondence: ghiath.jnido2@hawk.de; Tel.: +49-551-3705-291

check for updates

Abstract: In the present work, titanium dioxide (TiO$_2$) coatings were deposited on wood surfaces by an atmospheric pressure plasma jet using titanium tetraisopropoxide (TTIP) as a precursor to improve the wood's stability against ultraviolet (UV) light and its moisture resistance capability. The surface topology and morphology of the wood specimens were observed by scanning electron microscopy (SEM) and atomic force microscopy (AFM). Surface chemical compositions of the specimens were characterized by X-ray photoelectron spectroscopy (XPS) and by Fourier transform infrared (FTIR) spectroscopy. The wettability of the coated wood was investigated by measuring the sessile contact angle. SEM and AFM showed the presence of small globules of TiO$_2$ with some areas agglomerated on the coated wood surface. The coated surface roughness increased with increasing deposition time. FTIR analysis showed the existence of a Ti–O–Ti band at 800–400 cm^{-1} on the coated wood surfaces. The results obtained from FTIR were confirmed by XPS measurements. The hydrophilic wood surfaces were transformed to become hydrophobic or superhydrophobic after coating with TiO$_2$, depending on the deposition parameters. The changes of colour during UV-exposure for both uncoated and coated wood specimens were measured using the CIELab colour system. The TiO$_2$ coated wood became more resistant to colour change after UV radiation exposure than did untreated wood.

Keywords: atmospheric pressure plasma; coating; colour change; titanium dioxide; UV protection of wood; water resistance

1. Introduction

Wood is an organic material, consisting mainly of three compounds: cellulose, lignin and hemicelluloses [1]. When wood materials are used in outdoor applications, they are generally subjected to many weathering factors that affect their aesthetic appearance and mechanical performance, such as moisture, sunlight (especially ultraviolet (UV) radiation), and temperature (heat/cold). The untreated wood surface can be affected by the influence of sunlight in combination with rain, which leads to an initial discolouration followed by the destruction of mechanical and physical properties. Lignin, which is responsible for the characteristic colour changes, is the component most sensitive to UV light, since it undergoes structural changes in the presence of solar UV light and ultimately leads to discolouration and degradation of wood [2]. The discolouration of untreated wood surfaces is a serious aesthetic problem for many outdoor applications of wood such as garden furniture and facades [2,3]. Solar UV radiation that reaches the Earth's surface comprises approximately 95% UVA (315–400 nm) and 5% UVB (280–315 nm); all of UVC (100–280 nm) and most of UVB are filtered out by the Earth's atmosphere [4]. In order to improve the colour stability of wood, it is necessary to deposit thin protective barrier films on wood surfaces.

Some semiconductor metal oxides such as zinc oxide (ZnO) and titanium dioxide (TiO$_2$) are used to provide protection against the adverse effects of solar ultraviolet UVA and UVB radiation [5,6].

Titanium dioxide absorbs the UV photons because it has a suitable band gap between the electron-rich valence band and the electron-deficient conduction band, which can be overcome by the energy of UV photons [7,8]. The photocatalytic activity of TiO_2 depends on its crystalline phase. TiO_2 exists in nature in three crystalline phases: rutile (tetragonal structure), anatase (tetragonal structure) and brookite (orthorhombic structure). The rutile and anatase structures are the most common phases for applications. The anatase phase has a higher photocatalytic activity than the rutile phase due to the larger band gap (3.2 and 3.0 eV, respectively) [8]. Moreover, titanium dioxide has many other advantages. TiO_2 is biologically and chemically inert, photostable, inexpensive, of low toxicity, and it has good thermal stability [9]. Thus, TiO_2 can be used to improve wood surfaces against photodegradation caused by UV radiation, moisture, mould, fungus growth, stains and fire [10–17].

A number of methods have been developed to prepare coatings that improve the moisture and UV radiation resistance properties of wood and wood products, such as the sol gel method [18,19], hydrothermal methods of wood [11,12,20], and plasma-enhanced chemical vapor deposition (PECVD) [21,22]. In recent years, atmospheric pressure plasma technology has been used to deposit thin functional coatings on wood surfaces [6,15,18,21–23].

Atmospheric plasma deposition is an environmentally friendly and cost-effective technique for the synthesis of thin film materials with functional properties suitable for a wide range of applications [24]. This technique has many advantages, such as minimal chemical waste throughout the process, high processing speed, and flexibility in terms of its operation. It is a beneficial technology because vacuum equipment is not necessary, thereby allowing coatings to be deposited on substrates of any size and shape in ambient air without the need of a chamber. Furthermore, some atmospheric pressure plasma techniques that work at low temperature are suitable for the deposition of films on plastic and biological substrates [25,26].

Fakhouri et al. [27] reported the development of a simple and innovative method to deposit photocatalytic TiO_2 thin films at high rates with a high porosity on membranes by an open-air atmospheric pressure plasma jet (APPJ). This method is based on the spraying of a liquid precursor into a plasma jet (APPJ). Fakhouri et al. deposited the TiO_2 thin films on four different substrates and investigated the properties of these coatings, but they did not try to use this method for the preparation of TiO_2 coatings on wood.

In the present work, UV-protective TiO_2 thin films on wood substrates were deposited using an open air atmospheric pressure plasma jet (APPJ). The surface morphology and chemical compositions of the deposited TiO_2 coatings were investigated by scanning electron microscopy (SEM), atomic force microscopy (AFM), X-ray photoelectron spectroscopy (XPS), and by Fourier transform infrared (FTIR) spectroscopy. The superhydrophobic property of the coated specimens was measured by contact angle (CA) measurements. Discolouration of coated wood and wood control during the ultraviolet (UV) irradiation was periodically evaluated to compare the effect.

2. Materials and Methods

The experimental setup is described in Figure 1. TiO_2 coatings were deposited by using an atmospheric pressure plasma jet (APPJ) system from Reinhausen Plasma (Reinhausen Plasma GmbH, Regensburg, Germany) already used by several researchers [6,23]. Here, the plasma is generated in air at atmospheric pressure by employing a pulsed arc discharge. In order to generate the plasma, an ignition pulsed voltage of approximately 15 kV was applied between two tubular electrodes, with an effective voltage amounting to 2–3 kV. The pulse frequency of the discharge was 50 kHz with a duration of 5–10 µs, whereas the input power reached a maximum of 2 kW. Compressed air was used as the working gas. During the deposition, the working gas flow rate was fixed at 60 L/min. A spraying system (AGF 10.0, Palas GmbH, Karlsruhe, Germany) is attached to the plasma nozzle to introduce a solution precursor as spray into the plasma jet. Titanium tetraisopropoxide (TTIP, $Ti(OC_3H_7)_4$, 97%, Sigma Aldrich, Saint Louis, MO, USA) was used as the metalorganic precursor. The liquid precursor TTIP was nebulized with a cyclone (cut-off diameter of 10 µm), and sprayed into the plasma jet at

the nearest position to the outlet of the plasma nozzle. Nitrogen was used as a carrier gas to spray the precursor with a flow rate fixed at 14 L/min. In this study, to obtain the coatings, the specimens were moved by an xy-linear stage with velocities at 40 and 80 mm/s. The distance between the plasma nozzle and substrate was fixed at 24 mm.
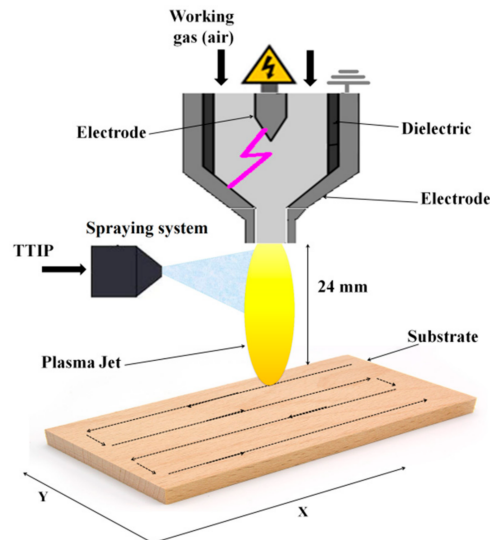

Figure 1. Schematic representation of the atmospheric pressure plasma jet (APPJ) system coupled with spraying system.

Specimens of defect-free beech wood were prepared with specimen sizes of 26 mm × 4 mm × 76 mm (width × height × length). All specimens were cut from the same board to ensure homogeneous characteristics for each specimen. Before deposition, the specimens were conditioned to 20 °C and 65% relative humidity for ten days in order to reach moisture equilibrium. In addition, some specimens of ordinary microscope glass slides were prepared for FTIR and AFM measurements.

In order to determine the UV-blocking efficiency of the TiO_2 coatings on wood, a UVA-365 lamp (Herolab GmbH, Wiesloch, Germany) with a maximum radiation wavelength of 365 nm was used. With an electrical input of 8 W, the lamp generates UV light with the intensity of 950 μW/cm^2. Eight wood specimens, each having a different coating, were exposed to UV light. The uncoated and TiO_2-coated specimens were irradiated with UVA light for a total of 100 h. Colour measurements were performed throughout the irradiation period at an interval of 10 h according to the CIELab system (see Figure 2). The experiments were carried out under ambient conditions at room temperature.
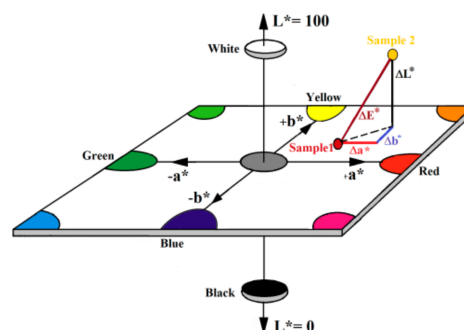

Figure 2. Graphical representation of the CIELab color space based on ref. [28].

The discolouration of wood surfaces due to UV irradiation was examined by taking pictures of the specimens using an EOS 600D digital camera (Canon Inc., Tokyo, Japan). All pictures were taken under equal conditions. For this purpose, the specimens were illuminated by using two parallel fluorescent

8 W lamps (length of 32.3 cm). The specimen illuminators and the camera were placed inside a black box to exclude external light and reflection. To ensure uniform illumination in the box, the illumination was measured by using the spectroradiometer CS-200A (Konica Minolta, Tokyo, Japan). A colour card (X-Rite Munsell ColorChecker, Grand Rapids, MI, USA) was used as a reference target. The pictures of the specimens were taken after each UV irradiation interval to analyze colour changes and to measure CIELab parameters by using the software Photoshop CS6.

The CIELab comprises the following three coordinates: The coordinate *L** represents the degree of colour lightness (ranging from 0 (black) to 100 (white)), while *a** and *b** are the chromatic coordinates of colour, where the +*a** value refers to red and the −*a** value to green while the +*b** and −*b** values refer to yellow and blue, respectively. The total colour change between two specimens was represented as the parameter Δ*E** calculated by the following equation:

$$\Delta E^* = (\Delta L^{*2} + \Delta a^{*2} + \Delta b^{*2})^{1/2} \tag{1}$$

where Δ means the difference between the indicated final and initial parameters after UV irradiation [28–30]. A low Δ*E** value means a small loss of colour and indicates that the specimens have a high resistance to damaging UV radiation.

The morphology of TiO_2 deposited by APPJ was characterized by scanning electron microscopy (SEM, Microscope JEOL JSM-5600LV, Tokyo, Japan, at 10 kV). The specimens were sputtered with a thin gold film (ca. 18 nm).

The surface morphology and roughness of the uncoated and TiO_2-coated specimens were studied using atomic force microscopy (AFM, Nanosurf Easy Scan2, Nanosurf AG, Liestal, Switzerland) in noncontact mode. The AFM-images were recorded in air at room temperature using silicon cantilevers (ACLA) with a spring constant of 58 N/m at a resonance frequency in the range of 160−225 kHz. Three-dimensional images were collected with a resolution of 512 points per line. The scan rate was 0.5 Hz. All obtained AFM topographic images were analyzed and processed by using the software Gwyddion (version 2.19) and the roughness average (R_a) of the scanned surface profiles was recorded.

The chemical analysis was performed by FTIR spectroscopy. The spectra were obtained by using a PerkinElmer Frontier spectrometer (Waltham, MA, USA) with an attenuated total reflectance (ATR) accessory (Golden Gate Single Reflection Diamond ATR, Specac, Orpington, UK) and by using the KBr pellet technique on a PerkinElmer Frontier spectrometer. Spectra were recorded over a range of 4000 to 400 cm^{-1}, and 64 scans were averaged at a resolution of 4 cm^{-1}.

X-ray photoelectron spectroscopy (XPS, PHI 5000 VersaProbe II, ULVAC-PHI, Chigasaki, Japan) using monochromatic Al Kα as an X-ray source with a photon energy of 1486.6 eV was performed to analyze the surface chemistry and elemental composition of the coated wood. The measurements were carried out at room temperature with a base pressure of 5×10^{-8} Pa. The measurement spot size of 200 μm in diameter was used for the analysis. Survey spectra were captured at a pass energy of 187.85 eV and detailed spectra at 23.5 eV with a step size of 0.1 eV for all spectra.

Water contact angle (WCA) measurements on the TiO_2-coated wood surfaces were carried out by using a measuring system G10 (Krüss GmbH, Hamburg, Germany) in order to investigate the hydrophobic properties of TiO_2 coatings. Droplets of distilled water with a volume of 11 μL were used for the contact angle measurements. The water droplets were recorded by a video camera for 10 s (25 frames/s) and the videos were analyzed by using the software DSA1 V1.9 (Krüss GmbH). The contact angle values were recorded 10 s after the placement of the water droplets on the wood surface.

3. Results and Discussion

3.1. Characterization of TiO_2 Coatings on Wood by Scanning Electron Microscopy (SEM)

The morphology of the TiO_2 coatings was observed by scanning electron microscopy (SEM) with a magnification of 2000×. The SEM images of the uncoated wood and the TiO_2-coated wood specimens prepared at different deposition velocities are shown in Figure 3. Figure 3a shows that the natural

wood specimen exhibited a smooth surface, while Figure 3b,c shows the growth of small globules of TiO_2 with some areas agglomerated on the wood surface, resulting in a rough surface. Figure 3b,c shows that both coated specimens have similar structures with different particle size and density distribution on the wood surfaces. It can be seen that the globules grow larger as the deposition velocity decreases, resulting in the compact and densely packed structure with a thicker coating. As shown in Figure 3b (velocity 80 mm/s), large agglomerates (~3 µm) with irregular shapes are common and much smaller agglomerates appear to be uniformly dispersed within the specimen. As shown in Figure 3c (velocity 40 mm/s), SEM observations confirmed that the coatings deposited with a velocity 40 mm/s were dense and large agglomerates (5–8 µm) with irregular shapes are common; much smaller agglomerates (~1 µm and smaller) appear to be uniformly dispersed within the specimen.
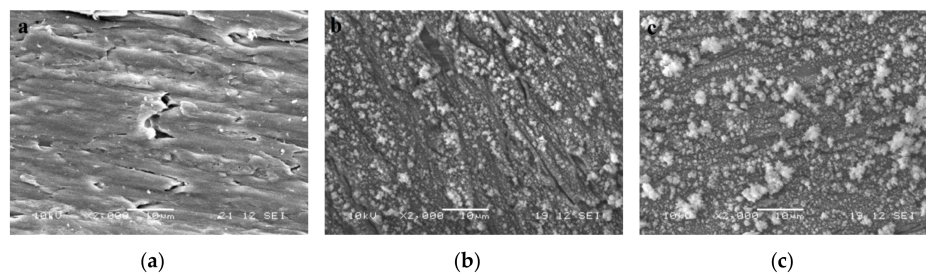

(**a**)   (**b**)   (**c**)

Figure 3. Scanning electron microscope (SEM) images of (**a**) uncoated wood and (**b**) TiO_2-coated wood at v = 80 mm/s, (**c**) TiO_2-coated wood at v = 40 mm/s.

3.2. Analysis of Surface Topography by Atomic Force Microscopy (AFM)

The surface topographies and roughness of the control and coated wood were further examined by AFM. The images were captured in the same position before and after deposition of plasma-polymerized TiO_2 on an area of 25 µm × 25 µm. The 3D AFM images are shown in Figure 4. Unlike the wood before coating, the coated substrates revealed the presence of small peaks on the surface, which was also apparent in SEM micrographs. The coated surfaces become sharper and rougher compared to uncoated surfaces (see Figure 4a–c). Due to the difficulty of ensuring that the values of the roughness of wood surfaces before and after film deposition were obtained in the same position, we measured the values of roughness from glass specimens which had been coated under the same conditions as the wood surfaces. It can be seen from the 3D AFM images that the roughness values (R_a) of coated surfaces increases from 215.1 to 271.6 nm with decreased deposition velocity from 80 to 40 mm/s (see Figure 4d–f). With increasing deposition time the surface roughness increases, indicating more growth of TiO_2 particles on the substrates.
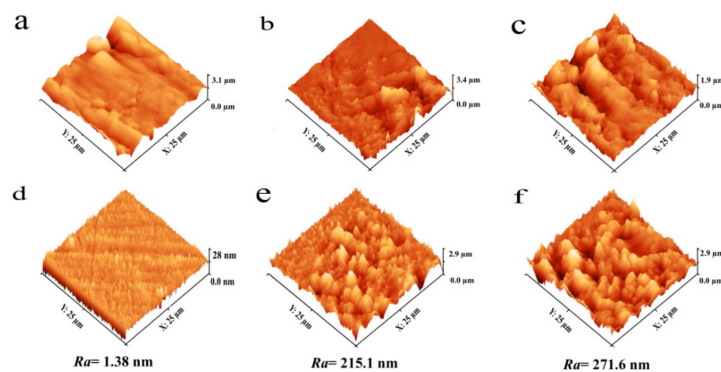

Figure 4. Three-dimensional atomic force microscopy (AFM) images of (**a**) uncoated wood, (**b**) TiO_2-coated wood at deposition velocity 80 mm/s, (**c**) TiO_2-coated wood at deposition velocity 40 mm/s, (**d**) uncoated glass, (**e**) TiO_2-coated glass at deposition velocity 80 mm/s and (**f**) TiO_2-coated glass at deposition velocity 40 mm/s.

3.3. Characterization of TiO₂ Coatings by Fourier Transform Infrared (FTIR) Spectroscopy

The chemical composition of the uncoated wood surface and the TiO_2-coated wood surface was examined with the infrared spectroscopy, as shown in Figure 5. From Figure 5a, it can be seen that the FTIR–ATR spectra of the coated wood were slightly different from that of the uncoated wood, probably because the ATR technique has a penetration depth around 5 µm, whereas the films have thicknesses smaller than 1 µm. The greatest obvious differences were the strengthening of the bands at 800–400 cm^{-1} for both coated specimens, indicating that the TiO_2 films had grown on the wood surface. The wide band at 800–400 cm^{-1} is attributed to the Ti–O–Ti stretch vibration [10–12,20]. Furthermore, the broad absorption band at 3333 cm^{-1} attributed to the O–H stretch vibration is slightly shifted to the lower wavenumbers of 3325 cm^{-1} after deposition of TiO_2 on the wood surface, probably due to the interaction between the hydroxyl groups of the wood surface and the deposited TiO_2 particles, which could result in the formation of chemical bonds (hydrogen bonding) at the interfaces of the wood surface and TiO_2 particles. However, Sun et al. reported that TiO_2 was chemically bonded to the wood surface through the combination of hydrogen groups during the hydrothermal process [12].
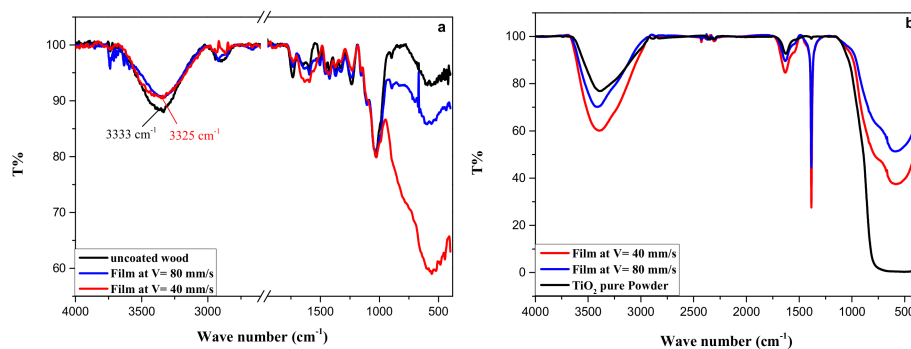

Figure 5. (**a**) Fourier transform infrared (FTIR) spectroscopy–attenuated total reflectance (FTIR–ATR) spectra for uncoated wood and TiO_2-coated wood; (**b**) Spectra for TiO_2 pure powder and TiO_2 powder scraped from the coated glass substrate.

It can be noted that the spectrum of the coated wood with lower deposition velocity has a stronger band at 800–400 cm^{-1} than that of the wood coated with higher deposition velocity, suggesting that the film was thicker with decreasing deposition velocity. These results were confirmed by SEM and AFM measurements.

To make sure that the band at 800–400 cm^{-1} is from titanium dioxide coatings, the coatings were also examined using the KBr Pellet technique to record FTIR spectra in transmission mode. For this purpose, some coatings were deposited onto glass substrates under the same conditions and parameters of the deposition onto wood substrates. The coatings were carefully scraped from the glass substrate to obtain powder specimens which were difficult to obtain from wood substrates without wood pieces. To prepare the KBr pellets, 1 mg of the scraped specimens was mixed with 300 mg of potassium bromide (KBr) salt and palletized under vacuum. Then, the pellets were investigated utilizing FTIR spectroscopy. The spectra obtained were compared to the spectrum of pure TiO_2 powder recorded under the same conditions. Figure 5b shows the FTIR spectra of the pure TiO_2 and the TiO_2 coatings scraped from the glass substrates. The band at 3375 cm^{-1} corresponds to the O–H stretching vibration of the hydroxyl groups. The band at 1629 cm^{-1} corresponds to the bending vibration of the –OH group [31–33]. The O–H-bands may be caused by hydroxyl groups on the surface of TiO_2 and adsorbed water. As can be seen, the commercial TiO_2 shows weaker bands and thus a smaller content of OH-groups. The long sharp band at 1384 cm^{-1} corresponds to NO_3^-, the presence of nitrate group in the spectra of coated specimens can be assumed as a result of plasma deposition in humid air [34,35]. The bands at 800–400 cm^{-1} could be attributed to the Ti–O–Ti stretch vibration [31–33].

3.4. Characterization of TiO₂ Coatings by X-ray Photoelectron Spectroscopy (XPS)

In addition, the surface chemical characteristics of the TiO_2 coating on wood surfaces were analyzed by XPS. Figure 6 shows the XPS survey spectra of uncoated and one of the TiO_2-coated wood surfaces. On the spectrum of uncoated wood, the presence of oxygen and carbon could be identified. For the coated specimen, titanium peaks and small amounts of nitrogen are recorded in addition to oxygen and carbon peaks, and the intensity of the oxygen peak increases significantly.
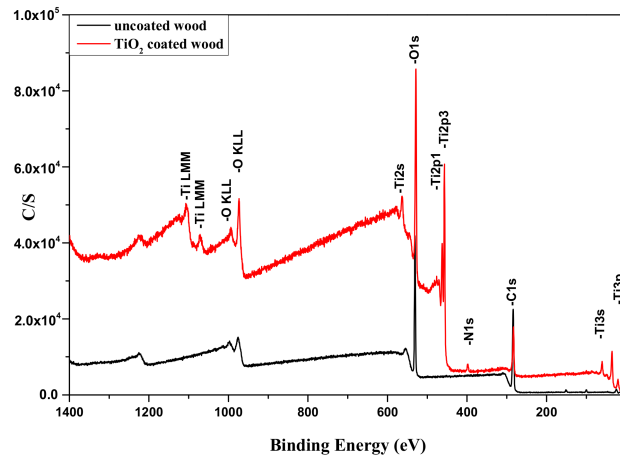

Figure 6. Survey spectra for uncoated (black) and TiO_2-coated wood (red) showing oxygen peaks and a carbon peaks and titanium peak.

In order to obtain information about the binding characteristics of the elements on the coated surface, high-resolution scans of the XPS spectra of the C 1*s*, O 1*s*, and Ti 2*p* region were analyzed. The spectra were fitted with symmetrical Gaussian/Lorentzian function and are shown in Figure 7. All binding energy values were determined by calibration and fixing the C 1*s* line to 284.8 eV.
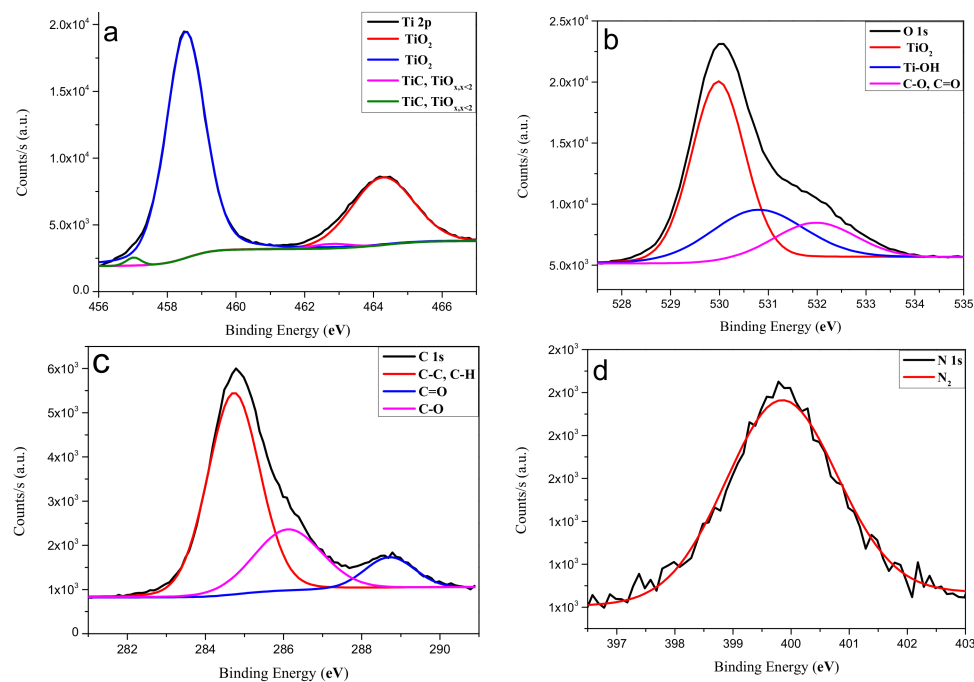

Figure 7. High-resolution XPS spectra of (**a**) Ti 2*p*, (**b**) O 1*s*, (**c**) C 1*s* and (**d**) N 1*s* of coated wood using Gaussian–Lorentzians deconvolution.

Figure 7a shows the Ti 2*p* high resolved spectrum which consists of doublet peaks of Ti 2$p_{1/2}$ and Ti 2$p_{3/2}$ located at binding energies of 458.5 and 464.3 eV, respectively. After the Ti 2*p* peak deconvolution, the two strong peaks Ti 2$p_{1/2}$ (464.31 eV) and Ti 2$p_{3/2}$ (458.53 eV) are assigned to Ti^{4+} (TiO$_2$ [27] and Ti–OH) and the two peaks (457.01 and 462.44 eV) are attributed to Ti$_2$O$_3$ [31].

The high-resolution spectrum of O 1*s* is shown in Figure 7b. The O 1*s* peak can be deconvoluted into three peaks located at 530.02, 531.59 and 532.75 eV, corresponding to Ti–O (TiO$_2$), Ti–OH and C–O or C=O, respectively [27,31,32,36].

The high-resolution spectrum of C 1*s* is shown in Figure 7c. The C 1*s* peak can be deconvoluted into three peaks: C–C at binding energy 284.71 eV, C–O at 286.03 eV, and C=O at binding energy 288.76 eV, respectively [27,31,32,36].

The high-resolution spectrum of N 1*s* is shown in Figure 7d. About 2 at.% of N was found throughout the specimens and is thus associated with bulk N originating from the air plasma and carrier gas N$_2$ [27].

The surface elements chemical state and atomic percentage of obtained coatings estimated from XPS spectra are given in Table 1. The elemental content of Ti was 16.48% and O was 45.59% with an atomic ratio (O/Ti = 2.76), which means that there are fewer oxygen atoms than in TTIP molecules (O/Ti = 4), but it is more than in TiO$_2$ compounds (O/Ti = 2). The deviation from the stoichiometric O/Ti ratio in XPS could be attributed to the presence of other formed oxygen functional groups e.g., OH-groups on the surface of the coating by air plasma deposition. The O/Ti ratio (as determined by XPS peak areas high-resolution scans O 1*s* at 530.01 eV and Ti 2$p_{1/2}$ at 458.53 eV and Ti 2$p_{3/2}$ at 464.31 eV) was two for this TiO$_2$ coating.

Table 1. Surface elements chemical state, peak position and atomic percentage from X-ray photoelectron spectroscopy (XPS) analysis.

Element	Binding Energy (eV)	Assignment	Atomic Percentage (at.%)
Ti	458.53 and 464.31	TiO$_2$	15.7
	457.01 and 462.44	Ti–C or TiO$_{x\,<\,2}$	0.8
O	530.01	TiO$_2$	31.3
	531.33	Ti–OH	10.8
	532.35	C–O or C=O	3.5
C	284.75	C–C or C-H	24.1
	286.18	C–O	8.3
	288.76	C=O	3.5
N	399.82	N$_2$	2.0

3.5. Ultraviolet (UV) Protection

To determine the UV-protection efficiency of TiO$_2$ coatings on the wood specimens, the wood specimens were exposed to UV irradiation for 100 h and their colour change was monitored over time. Nine measurements per specimen exposed to UV light were carried out for each interval of irradiation time and the average value was calculated. The results of the colour measurements of the coated and control wood specimens as a function of the UV irradiation time are given in Figure 8.
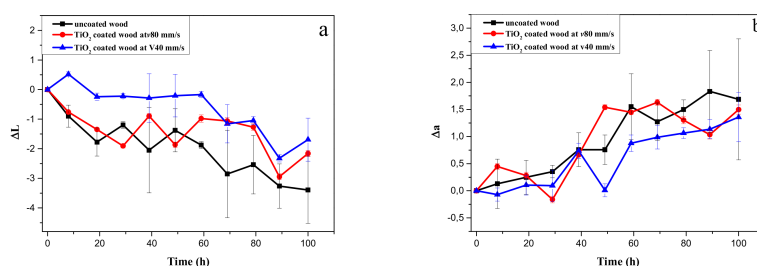

Figure 8. *Cont.*
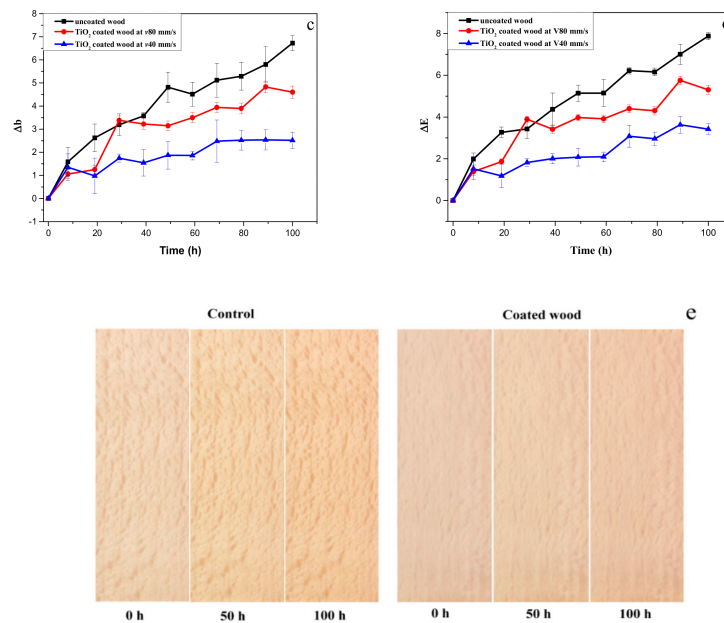
Figure 8. Colour change of coated and uncoated wood versus the irradiation time (**a**) lightness index change ΔL, (**b**) red-green index change Δa, (**c**) yellow-blue index change Δb, (**d**) total color change ΔE, and (**e**) optical images of the uncoated and coated wood before and after 50 and 100 h of irradiation.

As shown in Figure 8a, the ΔL^* value of both uncoated wood and TiO_2-coated wood decreased and became negative with increasing irradiation time, indicating that the surfaces of almost all the wood specimens became darker during the UV irradiation process. However, the ΔL^* value of the TiO_2-coated specimen at deposition velocity ($v = 40$ mm/s) decreased from 0 to −2 while that of the uncoated wood decreased from 0 to −3.5. The ΔL^* value of the TiO_2-coated specimen at deposition velocity ($v = 80$ mm/s) was not much different from that of the uncoated specimen. Generally, the ΔL^* value of all TiO_2-coated specimens was smaller than that of the untreated specimens.

As shown in Figure 8b, the Δa^* value of both uncoated wood and TiO_2-coated specimens increased with increasing irradiation time. However, the Δa^* value of the TiO_2-coated specimens had only a slight change compared to that of the untreated specimen. The increase in the Δa^* values indicated that the specimens turned a reddish colour with increasing UV irradiation time.

As shown in Figure 8c, the Δb^* value of both the uncoated specimen and the TiO_2-coated specimens increased with increasing irradiation time. However, the Δb^* change in TiO_2-coated specimens was smaller than that of the uncoated specimens. The Δb^* value of the TiO_2-coated specimens at deposition velocity ($v = 40$ mm/s) increased from 0 to 2.5 and from 0 to 4.6 for the TiO_2-coated specimens at deposition velocity ($v = 80$ mm/s), while the uncoated specimen increased from 0 to 6.7. The change in Δb^* value indicated that UV irradiation made the wood surface of the uncoated and TiO_2-coated specimens increasingly yellowish; the colours turned a dark yellow and slightly yellow for uncoated and TiO_2-coated specimens, respectively, with increasing UV irradiation time. The colour change of the TiO_2-coated specimens at deposition velocity ($v = 40$ mm/s) showed the best colour stability. The difference in the total colour variation between the coated specimen at deposition velocity ($v = 80$ mm/s) and the uncoated specimen was insignificant, but the ΔE^* value was still smaller than the value of the uncoated specimens.

The total colour change ΔE^* curves are shown in Figure 8d. It can be seen that the total colour change of all the wood specimens increased with increasing UV irradiation time. The TiO_2-coated specimens showed less colour change than the uncoated specimens; the ΔE^* value of the TiO_2-coated specimens at deposition velocity ($v = 40$ mm/s) increased from 0 to 3.4 and from 0 to 5.3 for the TiO_2-coated specimens at deposition velocity ($v = 80$ mm/s), while the uncoated specimen increased from 0 to 7.8 after the 100 h UV irradiation test. The colour change of the TiO_2-coated specimens at

deposition velocity (v = 40 mm/s) showed better colour stability than that of the coated specimens at deposition velocity (v = 80 mm/s).

The photograph in Figure 8e shows the colour change of wood for the uncoated and TiO$_2$-coated specimens at deposition velocity (v = 40 mm/s) after 50 and 100 h of exposure. Here, we can note that TiO$_2$-coated wood is more stable during 100 h of UV irradiation than uncoated wood.

According to George et al. [37] the component lignin undergoes photo-oxidation under UV light forming carbonyl-based chromophoric compounds. This leads to a discolouration of irradiated wood surfaces. The absorption of UV light by the TiO$_2$ coating resulted in the UV intensity decreasing when it reached the wood components. Thus the oxidation processes of the TiO$_2$-coated wood slowed down. Schulte [38] reported a micronized titanium dioxide powder used as a UV absorber to photostabilize wood surfaces. The ability of TiO$_2$ coatings to protect against UV light was also reported by Rassam et al. [10], Sun et al. [12] and Zheng et al. [15]. Based on the results of the present study, the TiO$_2$-coated wood had more UV resistance than uncoated wood and thus the wood surface was better protected from damage. A similar protection effect was reported by Wang et al. [18].

3.6. Contact Angle Analysis (Water)

The hydrophobicity of the wood surfaces was evaluated by water contact angle (WCA) measurements. Images of water droplets on the wood surfaces are shown in Figure 9. As anticipated, the untreated wood surface was hydrophilic and had an average WCA of 73° as shown in Figure 9a. However, the average WCA on the coated wood surface was 83° for the specimens deposited at v = 80 mm/s (Figure 9b) and the average WCA reached 150° for the specimens deposited at v = 40 mm/s (Figure 9c). Thus, the introduction of the TiO$_2$ coatings on the wood substrate improved water repellency, transforming the wood surface from hydrophilic to hydrophobic or superhydrophobic depending on the deposition parameters. The TiO$_2$ coatings deposited at v = 80 mm/s are not very thick on the wood specimens, as was shown in the SEM images. Nevertheless, the coatings are partially able to protect the wood from water.
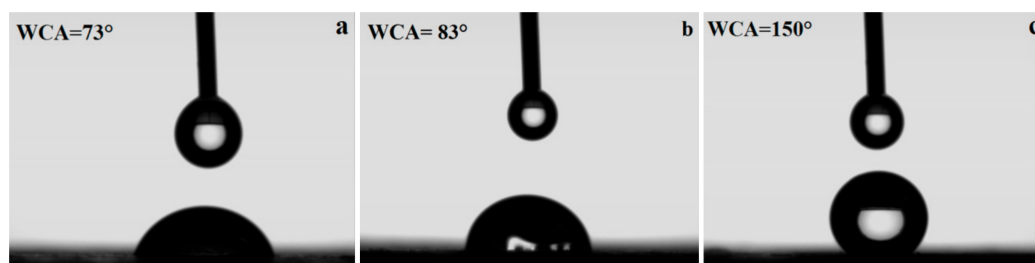

Figure 9. Images of 11 μm water droplets on (**a**) uncoated wood, (**b**) TiO$_2$-coated wood surface at v = 80 mm/s and (**c**) TiO$_2$-coated wood surface at v = 40 mm/s.

The achieved high water repellency can be attributed to the combined effects of the TiO$_2$ with wood and the surface roughness of coated wood. By plasma polymerization, the hydroxyl groups produced from polymerized TTIP react with the hydroxyl groups of wood and water adsorbed on the wood surface and thus the hydrophobicity property of the surface was created. According to the Wenzel model, it is necessary to increase the surface roughness of the substrate to achieve high hydrophobicity of surfaces [39,40]. The deposition of TiO$_2$ coatings on the wood surface facilitates the formation of high roughness on the wood substrate. Therefore, it contributed to the increase of the water contact angle.

After exposure to UV illumination, the TiO$_2$-coated wood surfaces switched to superhydrophilic (WCA, approximately 0°) and gradually returned to a more hydrophobic state (WCA, approximately 50°) with storage in the dark for 10 days. This phenomenon can be related to the photocatalytic activity of TiO$_2$ under UV irradiation [9,41]. This control of the switchable surface wetting would

be beneficial for enhanced applications, e.g., in the self-cleaning [41] and antifungal properties for wood surfaces [42].

According to Fakhouri et al. [27], the TiO_2 coatings deposited by APPJ revealed good adhesion to the substrates. But in our case (our coating parameters), the TiO_2 coatings on the wooden substrate revealed relatively poor adhesion to the substrate. Subsequent work is required to improve the stability of the TiO_2 coatings on wood surfaces obtained by the deposition method described here.

4. Conclusions

SEM and AFM results showed that TiO_2 thin films have been successfully deposited on wood surfaces using a plasma polymerization method by atmospheric pressure plasma jet (APPJ). The particle size and the roughness of the wood surface increased as a result of increasing deposition time. The analysis of XPS and FTIR spectra of the coated and uncoated wood demonstrates that the wood surface was covered with TiO_2 particles.

Plasma polymerized TiO_2 coatings improved the water repellency of wood surfaces; the wood surfaces were transformed after coating from hydrophilic to hydrophobic or superhydrophobic, depending on the deposition parameters.

The wood surface after coating with TiO_2 had more resistance to colour change after exposure to UV radiation than untreated wood; thus the wood surface was protected from damage for use in outdoor applications.

Additional research is required to improve the stability of the TiO_2 coatings on wood surfaces in order to improve the weathering performance of wood.

References

1. Fengel, D.; Wegener, G. *Wood Chemistry, Ultrastructure, Reactions*; Walter de Gruyter: Berlin, Germany, 1984.
2. Feist, W.C.; Hon, D.S. Chemistry of weathering and protection. In *The Chemistry of Solid Wood*; Rowell, R.M., Ed.; American Chemical Society: Washington, DC, USA, 1984; Volume 207, pp. 401–451.
3. Garcia, R.A.; Lopes, J.O.; Nascimento, A.M.; Latorraca, J.V. Color stability of weathered heat-treated teak wood. *Maderas Cienc. Tecnol.* **2014**, *16*, 453–462. [CrossRef]
4. Diffey, B.L. Sources and measurement of ultraviolet radiation. *Methods* **2002**, *28*, 4–13. [CrossRef]
5. Yang, H.; Zhu, S.; Pan, N. Studying the mechanisms of titanium dioxide as ultraviolet-blocking additive for films and fabrics by an improved scheme. *J. Appl. Polym. Sci.* **2004**, *92*, 3201–3210. [CrossRef]
6. Wallenhorst, L.; Gurău, L.; Gellerich, A.; Militz, H.; Ohms, G.; Viöl, W. UV-blocking properties of Zn/ZnO coatings on wood deposited by cold plasma spraying at atmospheric pressure. *Appl. Surf. Sci.* **2018**, *434*, 1183–1192. [CrossRef]
7. Liu, X.H.; Fu, Y.B. Studies on the structures and optical properties of TiO_2 doped with transition metals. In Proceedings of the 8th Pacific Rim International Congress on Advanced Materials and Processing, Waikoloa, HI, USA, 4–9 August 2013; pp. 295–305.
8. Linsebigler, A.L.; Lu, G.; Yates, J.T. Photocatalysis on TiO_2 surfaces: Principles, mechanisms, and selected results. *Chem. Rev.* **1995**, *95*, 735–758. [CrossRef]
9. Hashimoto, K.; Irie, H.; Fujishima, A. TiO_2 photocatalysis: A historical overview and future prospects. *Jpn. J. Appl. Phys.* **2005**, *44*, 8269–8285. [CrossRef]
10. Rassam, G.; Abdi, Y.; Abdi, A. Deposition of TiO_2 nano-particles on wood surfaces for UV and moisture protection. *J. Exp. Nanosci.* **2011**, *7*, 468–476. [CrossRef]

11. Li, J.; Yu, H.; Sun, Q.; Liu, Y.; Cui, Y.; Lu, Y. Growth of TiO_2 coating on wood surface using controlled hydrothermal method at low temperatures. *Appl. Surf. Sci.* **2010**, *256*, 5046–5050. [CrossRef]

12. Sun, Q.; Lu, Y.; Zhang, H.; Zhao, H.; Yu, H.; Xu, J.; Fu, Y.; Yang, D.; Liu, Y. Hydrothermal fabrication of rutile TiO_2 submicrospheres on wood surface: An efficient method to prepare UV-protective wood. *Mater. Chem. Phys.* **2012**, *133*, 253–258. [CrossRef]

13. Sun, Q.; Yu, H.; Liu, Y.; Li, J.; Cui, Y.; Lu, Y. Prolonging the combustion duration of wood by TiO_2 coating synthesized using cosolvent-controlled hydrothermal method. *J. Mater. Sci.* **2010**, *45*, 6661–6667. [CrossRef]

14. Sun, Q.; Yu, H.; Liu, Y.; Li, J.; Lu, Y. Improvement of water resistance and dimensional stability of wood through titanium dioxide coating. *Holzforschung* **2010**, *64*, 757–761. [CrossRef]

15. Zheng, R.; Tshabalala, A.M.; Li, Q.; Wang, H. Construction of hydrophobic wood surfaces by room temperature deposition of rutile (TiO_2) nanostructures. *Appl. Surf. Sci.* **2015**, *328*, 453–458. [CrossRef]

16. Zanatta, P.; Lazarotto, M.; Cademartori, P.H.; Cava, S.; Moreira, M.; Gatto, D. The effect of titanium dioxide nanoparticles obtained by microwave-assisted hydrothermal method on the color and decay resistance of pinewood. *Maderas Cienc. Tecnol.* **2017**, *19*, 495–506. [CrossRef]

17. Miyafuji, H.; Saka, S. Fire-resisting properties in several TiO_2 wood-inorganic composites and their topochemistry. *Wood Sci. Technol.* **1997**, *31*, 449–455. [CrossRef]

18. Wang, X.Q.; Liu, S.C.; Chang, H.J.; Liu, J.L. Sol-gel deposition of TiO_2 nanocoatings on wood surfaces with enhanced hydrophobicity and photostability. *Wood Fiber Sci.* **2014**, *46*, 109–117.

19. Hübert, T.; Unger, B.; Bücker, M. Sol-gel derived TiO_2 wood composites. *J. Sol-Gel Sci. Technol.* **2010**, *53*, 384–389. [CrossRef]

20. Pavel, P.; Aljaž, V.; Marko, P.; Andrijana, S.; Mohor, M.; Angela, S.; Urban, N.; Boris, O. Structural studies of TiO_2/wood coatings prepared by hydrothermal deposition of rutile particles from $TiCl_4$ aqueous solutions on spruce (*Picea Abies*) wood. *Appl. Surf. Sci.* **2016**, *372*, 125–138.

21. Levasseur, O.; Stafford, L.; Gherardi, N.; Naudé, N.; Blanchard, V.; Blanchet, P.; Riedl, B.; Sarkissian, A. Deposition of hydrophobic functional groups on wood surfaces using atmospheric-pressure dielectric barrier discharge in helium hexamethyldisiloxane gas mixtures. *Plasma Process. Polym.* **2012**, *9*, 1168–1175. [CrossRef]

22. Gerullis, S.; Pfuch, A.; Spange, S.; Kettner, F.; Plaschkies, K.; Kosmachev, P.V.; Volokitin, G.; Grünler, B. Antimicrobial coatings on wood by use of atmospheric pressure chemical vapour deposition (APCVD). *Holztechnologie* **2016**, *57*, 16–25.

23. Köhler, R.; Sauerbier, P.; Militz, H.; Viöl, W. Atmospheric pressure plasma coating of wood and MDF with polyester powder. *Coatings* **2017**, *7*, 171. [CrossRef]

24. Buske, C. Environmentally friendly and cost-saving Atmospheric-pressure plasma technology. *Innov. Surf. Technol.* **2009**, *2*, 18–22.

25. Dong, S.; Zhao, Z.; Dauskardt, R.H. Highly transparent bilayer organosilicate multifunctional coatings on plastics deposited by atmospheric plasma deposition with dual organic and inorganic precursors in air. *ACS Appl. Mater. Interf.* **2015**, *7*, 17929–17934. [CrossRef] [PubMed]

26. Pappas, D. Status and potential of atmospheric plasma processing of materials. *J. Vac. Sci. Technol. A Vac. Surf. Films* **2011**, *29*, 020801. [CrossRef]

27. Fakhouri, H.; Ben Salem, D.; Carton, O.; Pulpytel, J.; Arefi-Khonsari, F. Highly effcient photocatalytic TiO_2 coatings deposited by open air atmospheric pressure plasma jet with aerosolized TTIP precursor. *J. Phys. D Appl. Phys.* **2014**, *47*, 265301. [CrossRef]

28. Mokrzycki, W.S.; Tatol, M. Colour difference ΔE—A survey. *J. Mach. Graph. Vis.* **2011**, *20*, 383–411.

29. Ozen, E.; Yeniocak, M.; Colak, M.; Koca, I. Colorability of wood material with punica granatum and morus nigra extracts. *Bioresources* **2014**, *9*, 2797–2807. [CrossRef]

30. Oberhofnerová, E.; Pánek, M.; García-Cimarras, A. The effect of natural weathering on untreated wood surface. *Maderas Cienc. Tecnol.* **2017**, *19*, 173–184. [CrossRef]

31. Chen, Q.; Liu, Q.; Hubert, J.; Huang, W.; Baert, K.; Wallaert, G.; Terryn, H.; Delplancke-Ogletree, M.; Reniers, F. Deposition of photocatalytic anatase titanium dioxide films by atmospheric dielectric barrier discharge. *Surf. Coat. Technol.* **2017**, *310*, 173–179. [CrossRef]

32. Olay, M.G.; González-Salgado, F.; Cruz, G.J.; Gómez, L.; García-Rosales, G.; Gonzalez-Torres, M.; Lopez-Gracia, O.G. Chemical structure of TiO organometallic particles obtained by plasma. *Adv. Nanopart.* **2013**, *2*, 229–235. [CrossRef]

33. Nakamura, M.; Korzec, D.; Aoki, T.; Engemann, J.; Hatanaka, Y. Characterization of TiO$_x$ film prepared by plasma enhanced chemical vapor deposition using a multi-jet hollow cathode plasma source. *Appl. Surf. Sci.* **2001**, *175*, 697–702. [CrossRef]

34. Borca, E.; Bercu, M.; Georgescu, S.; Hodorogea, S.; Cotoi, E. XRD and FTIR characterization of nanocrystalline YVO$_4$:Eu derived by coprecipitation process. *Z. Krist. Suppl.* **2008**, *27*, 457–462.

35. Dou, B.; Wang, Y.; Zhang, T.; Liu, B.; Shao, Y.; Meng, G.; Wang, F. Growth behaviors of layered double hydroxide on microarc oxidation film and anti-corrosion performances of the composite film. *J. Electrochem. Soc.* **2016**, *163*, 917–927. [CrossRef]

36. Kang, S.; Mauchauffé, R.; You, Y.S.; Moon, S.Y. Insights into the role of plasma in atmospheric pressure chemical vapor deposition of titanium dioxide thin films. *Sci. Rep.* **2018**, *8*, 16684. [CrossRef] [PubMed]

37. George, B.; Suttie, E.; Merlin, A.; Deglise, X. Photodegradation and photostabilisation of wood—The state of the art. *Polym. Degrad. Stab.* **2005**, *88*, 268–274. [CrossRef]

38. Schulte, K. Application of micronized titanium dioxide as inorganic UV absorber. In Proceedings of the 11th Asia Pacific Coating Conference, Bangkok, Thailand, 26–27 June 2001.

39. Wenzel, R.N. Surface roughness and contact angle. *J. Phys. Colloid Chem.* **1949**, *53*, 1466–1467. [CrossRef]

40. Momen, G.; Farzaneh, M.; Nekahi, A. Properties and applications of superhydrophobic coatings in high voltage outdoor insulation: A review. *IEEE Trans. Dielectr. Electr. Insul.* **2017**, *24*, 3630–3646.

41. Gao, L.; Lu, Y.; Cao, J.; Li, J.; Sun, Q. Reversible photocontrol of wood-surface wettability between superhydrophilicity and superhydrophobicity based on a TiO$_2$ film. *J. Wood Chem. Technol.* **2015**, *35*, 365–373. [CrossRef]

42. Chen, F.; Yang, X.; Wu, Q. Antifungal capability of TiO$_2$ coated film on moist wood. *Build. Environ.* **2009**, *44*, 1088–1093. [CrossRef]